Increasing the robustness of fault identification in rotor dynamics by means of M-estimators

Paolo Pennacchi*, Andrea Vania, Nicolò Bachschmid
Department of Mechanics
Politecnico di Milano
Via La Masa, 34, I-20156, Milan, Italy
paolo.pennacchi@polimi.it, andrea.vania@polimi.it, nicolo.bachschmid@polimi.it

ABSTRACT

One of the most common problems in rotor dynamics is the identification of faults and model based methods are often used. In some applications, the least squares (LS) estimate is used to find out the position and the severity of impending faults on the basis of experimental vibration data of rotating machinery. Anyhow LS are not very robust with respect to possible outliers (noise and gross errors) in the experimental data and to inaccuracies in the model.

The introduction of weights in the LS algorithm has proven to be effective to increase the robustness and successful experimental cases, both on test rigs and real machines, are reported in literature. However the arbitrary choice of the weights is normally based on operators' experience. In this paper an improvement is presented by introducing a method that is robust by itself, the M-estimate, which allows defining automatically the weights. This method is general and can be applied in every problem of regression or estimation, not necessarily related to rotor dynamics.

The fundamental theoretical aspects are introduced in the first part, while several experimental test-cases are presented by means of fault identification on a test-rig and on a gas turbo-generator in the second part of the paper. The obtained results highlight the increasing of the accuracy allowed by M-estimate.

KEY WORDS

Robust estimation, M-estimator, Identification, Diagnostics, Rotor dynamics, Unbalance.

1 INTRODUCTION

It is well known that least squares (LS) estimate can badly behave when the error distribution is not normal, particularly when the errors are heavy-tailed [29]. One remedy is to remove influential and corrupting observations from the least squares fit or to use weighted least squares [11]. These operations should be normally performed by skilled operators, since the deletion or the attribution of weights is rather arbitrary.

The advantages of the implementation of a robust technique are that the experimental data do not need to be inspected in order to check for the presence of corrupting noise or gross errors.

A suitable approach is the use of robust regression [16], i.e. the employing of a fitting criterion that is not as vulnerable as least squares to outlying data and contemporary it is able to indicate the possible inaccuracies in the model of the system.

* Corresponding author. Tel.: +39-02-2399.8440; fax: +39-02-2399.8492.

The paper proposes the implementation of the robust regression by using the M-estimators: the standard LS method tries to minimize the sum of the square residuals of every data. Outlying data give an effect so strong in the minimization that the estimated parameters are distorted. The M-estimators try to reduce the effects of the outliers by replacing the square of the errors by another function of them. Several functions of the errors have been proposed [29], but whatever is chosen, the implementation is made by using iteratively the re-weighted least squares (IRLS) algorithm. Practically, the algorithm recursively assign weights to data in order to minimize the effect of outliers. Whilst M-estimate is used in many different field after its introduction in statistics, like image recognition (i.e. [28][29]), electrical power systems (i.e. [15]) or chemical engineering (i.e. [18]), there are not application on mechanical systems. A possible explanation could be that the analytical methods developed in statistics, and applied on the other fields, handle data that are composed by real numbers, while often experimental data of mechanical systems are vibrations that can be suitably represented by means of complex numbers, i.e. amplitude and phase. In this paper, the authors introduce the M-estimate applied to identification of mechanical systems, especially to rotor dynamics. A preliminary analysis [5] has been already performed to select the most suitable type of M-estimator to be applied to mechanical systems.

In order to show the effectiveness and the performances of the proposed method, the paper presents several experimental cases of balancing mass identification in a test rigs and in an industrial machine, showing the increasing of the accuracy in the estimation of the unbalance.

2 GENERAL APPROACH TO MODEL BASED IDENTIFICATION OF FAULT IN THE FREQUENCY DOMAIN FOR ROTOR SYSTEM

The model based identification of faults in rotor systems is essentially a MIMO (multiple inputs, multiple outputs) inverse problem. Some applications in rotor dynamics have been presented in both the time domain [23] and the frequency domain. Multiple faults can be considered as inputs and the vibrations, measured in different planes along two orthogonal directions, are the multiple outputs. Previous papers of the same authors ([3][4][20]) have shown how to define the model of the system and the model of common faults in rotor dynamics by means of equivalent excitation systems.

With regards to the experimental data, *additional vibrations* are used. They are obtained by means of the difference between the faulty condition and the reference condition. Under the hypothesis of linearity of the system, which is satisfied in many cases of common faults in rotating machinery, the additional vibrations are caused by the developing faults only. Further discussion about this topic can be found in [19][21].

Anyhow, since many types of faults of rotating machinery have effect, and thus related symptoms are acting, on few harmonic components (as well known in literature starting from Sohre's chart), the harmonic balance approach is used. The following equations are obtained for each harmonic component, in which the equivalent excitation vector $\mathbf{F}_{f_n}$, has to be identified:

$$\left[-(n\Omega)^2[\mathbf{M}]+in\Omega[\mathbf{C}(\Omega)]+[\mathbf{K}]\right]\mathbf{X}_n=\mathbf{F}_{f_n} \tag{1}$$

where $[\mathbf{M}]$ is the mass matrix, $[\mathbf{C}(\Omega)]$ is the complete damping matrix that includes also the gyroscopic matrix calculated at the speed Ω, $[\mathbf{K}]$ is the stiffness matrix.

Because the system is considered as linear, the effect of m faults developing simultaneously can be considered by means of the superposition of the effects for each harmonic component:

$$\mathbf{F}_{f_n} = \sum_{i=1}^{m} \mathbf{F}_{f_n}^{(i)} \tag{2}$$

These are the multiple inputs (MI) of the system. Moreover, the k-th fault acts on few degrees of freedom (d.o.f.s) of the system, therefore the vector $\mathbf{F}_{f_n}^{(k)}$ is not a full-element vector which is convenient to be represented by means of:

$$\mathbf{F}_{f_n}^{(k)} = \left\{\mathbf{F}_L^{(k)}\right\} \theta^{(k)}(\Omega), \quad \theta^{(k)}(\Omega) \in \mathbb{C} \tag{3}$$

where $\left\{\mathbf{F}_L^{(k)}\right\}$ is the localisation vector which has all null-elements, except for the d.o.f.s to which the exciting system is applied, and $\theta^{(k)}(\Omega)$ is a complex number representing the amplitude and the phase of the fault. Obviously, as many nodes are used for the model, as much the location of the fault is accurate.

In the paper, in which unbalances are going to be identified, it is sufficient to consider the 1x rev. component of the vibration, but the method can be easily modified for other fault types, by using the corresponding fault model. Since the unbalance can be only applied on the rotor nodes and not to the foundation, the k-th unbalance can be expressed as:

$$\mathbf{F}_{f_1}^{(k)} = \left\{0 \ \vdots \ \underbrace{1 \ \ 0 \ \ i \ \ 0}_{j\text{-th rotor node}} \ \vdots \ 0 \ \ \underbrace{0 \ \cdots \ 0}_{\text{foundation d.o.f.s}}\right\}^{\mathrm{T}} \cdot \left(mr\right)^{(k)} \Omega^2 e^{i\varphi^{(k)}} = \Omega^2 \left\{\mathbf{F}_L^{(k)}\right\} \theta^{(k)} \tag{4}$$

In eq. (4) the only elements different from zero are those relative to the horizontal and vertical d.o.f.s of the node *j*, where the unbalance is supposed to be applied.

In general, the monitoring data used to identify the fault are collected for many rotating speeds and on different measuring planes (which often are corresponding to the bearings). The rotating speeds, at which the additional vibrations are available, are organized as a vector of n_p elements:

$$\mathbf{\Omega} = \left\{\Omega_1 \quad \Omega_2 \quad \ldots \quad \Omega_{n_p}\right\}^{\mathrm{T}} \tag{5}$$

If the measuring planes are l, the experimental vibrations are measured along two orthogonal directions per each plane and the vector of the additional vibrations is organized as follows:

$$\mathbf{\Xi} = \left\{\xi_V^{(1)}(\Omega_1) \ \xi_H^{(1)}(\Omega_1) \cdots \xi_V^{(l)}(\Omega_1) \ \xi_H^{(l)}(\Omega_1) \quad \cdots \quad \xi_V^{(1)}(\Omega_{n_p}) \ \xi_H^{(1)}(\Omega_{n_p}) \cdots \xi_V^{(l)}(\Omega_{n_p}) \ \xi_H^{(l)}(\Omega_{n_p})\right\}^{\mathrm{T}} \tag{6}$$

where e.g. $\xi_V^{(1)}(\Omega_1)$ indicates the vertical vibration in the 1st measuring plane, evaluated at the rotating speed Ω_1.

These are the measured multiple outputs (MO) of the considered system. Then, introducing the admittance matrix of the system and dropping the subscript index n of the harmonic component order for simplicity, eq. (1) becomes:

$$\left[\mathbf{Z}(\mathbf{\Omega})\right] \ \mathbf{X}(\mathbf{\Omega}) = \begin{bmatrix} \mathbf{Z}(\Omega_1) & 0 & 0 & 0 \\ 0 & \mathbf{Z}(\Omega_2) & 0 & 0 \\ \vdots & \vdots & \vdots & \vdots \\ 0 & 0 & 0 & \mathbf{Z}(\Omega_{n_p}) \end{bmatrix} \begin{Bmatrix} \mathbf{X}(\Omega_1) \\ \mathbf{X}(\Omega_2) \\ \vdots \\ \mathbf{X}(\Omega_{n_p}) \end{Bmatrix} = \begin{Bmatrix} \sum_{i=1}^{m} \mathbf{F}_f^{(i)}(\Omega_1) \\ \sum_{i=1}^{m} \mathbf{F}_f^{(i)}(\Omega_2) \\ \vdots \\ \sum_{i=1}^{m} \mathbf{F}_f^{(i)}(\Omega_{n_p}) \end{Bmatrix} = \mathbf{F}_f(\mathbf{\Omega}) \tag{7}$$

If the rotor model has n_r nodes and the support structure is represented by means of a foundation with k_m d.o.f.s, the d.o.f.s of fully assembled model are $(4n_r + k_m)$, while only $2l$ d.o.f.s are measured per each rotating speed. The admittance matrix $\left[\mathbf{Z}(\boldsymbol{\Omega})\right]$ has order $\left((4n_r + k_m)n_p \times (4n_r + k_m)n_p\right)$.

The equivalent excitation system, for each one of the m faults considered, is repeated for all the rotating speed so that the fault vector is of order $\left((4n_r + k_m)n_p\right) \times m$; taking into account that in this case the unbalance is considered, in order to eliminate the dependence on the rotating speed square that appear in eq. (4), it is convenient to insert Ω_j^2 in the localization vector of each rotating speed. Therefore, in the first node, the localization vector of the k-th fault, for the j-th rotating speed is:

$$\left\{\underline{\mathbf{F}}_L^{(k),(j)}\right\} = \Omega_j^2 \left\{ \underbrace{1 \;\; 0 \;\; i \;\; 0}_{1^{st}\text{ node}} \;\; \underbrace{0 \;\; 0 \;\; 0 \;\; 0}_{2^{nd}\text{ node}} \;\; \vdots \;\; \underbrace{0 \;\; 0 \;\; 0 \;\; 0}_{n_r^{th}\text{ node}} \;\; \underbrace{0 \;\; \ldots \;\; 0}_{k_m\text{ d.o.f.s}} \right\}^{\mathrm{T}} \tag{8}$$

and for all the n_p rotating speeds:

$$\mathbf{F}_L^{(k)} = \left\{ \left\{\underline{\mathbf{F}}_L^{(k),(1)}\right\} \;\; \cdots \;\; \left\{\underline{\mathbf{F}}_L^{(k),(n_p)}\right\} \right\}^{\mathrm{T}} \tag{9}$$

Since the faults have to be identified not only in their severity but also in their position, the identification procedure starts by assuming the positions as known, then identifies the corresponding amplitudes and phases. All the subsequent permutations of fault number and position have to be evaluated, unless the research of the faults is limited inside a specified interval of the nodes. The permutations ${}_{n_r}P_m$ are indicated by the subscript so that $(1,5,\ldots)$ means that the first excitation is applied in node 1, the second in node 5, etc. These iterations are implemented in one loop. In the first step of the loop, all the equivalent excitations are supposed to be in the first node.

The effect on the measured d.o.f.s, due to all the exciting systems applied to the first node on the model and assumed to have unitary value ($\theta^{(k)} = 1, \forall k$), is the vector $\left[\mathbf{Y}_{(1,\cdots,1)}\right]$ of order $(2l\, n_p \times m)$. Following the statistical nomenclature, $\left[\mathbf{Y}_{(1,\cdots,1)}\right]$ is the model matrix. The k-th column of the vector corresponds to the effect of the k-th generalized force. The calculation of $\left[\mathbf{Y}_{(1,\cdots,1)}\right]$ is done first by substituting eq. (9) in the right hand side of eq. (7), and inverting matrix $\left[\mathbf{Z}(\boldsymbol{\Omega})\right]$, obtaining the matrix $\left[\mathbf{H}(\boldsymbol{\Omega})\right]$.

$$\mathbf{X} = \left[\mathbf{Z}\left(\boldsymbol{\Omega}\right)\right]^{-1} \mathbf{F}_L(\boldsymbol{\Omega}) = \left[\mathbf{H}\left(\boldsymbol{\Omega}\right)\right] \mathbf{F}_L(\boldsymbol{\Omega}) \tag{10}$$

Then, the vibrations of the d.o.f.s that are measured, are separated from all the d.o.f.s of the system, by considering only the rows of $\left[\mathbf{H}(\boldsymbol{\Omega})\right]$ corresponding to the measured d.o.f.s. The partitioned matrix $\left[\underset{\sim}{\mathbf{H}}(\boldsymbol{\Omega})\right]$ is of order $\left(2l\, n_p \times (4n_r + k_m)n_p\right)$ and results:

$$\left[\mathbf{Y}_{(1,\ldots,1)}\right] = \left[\underset{\sim}{\mathbf{H}}\left(\boldsymbol{\Omega}\right)\right] \left[\mathbf{F}_L^{(1)} \;\; \vdots \;\; \mathbf{F}_L^{(m)}\right] \tag{11}$$

Now the array $\boldsymbol{\theta}$, which is of order $(m \times 1)$, of the complex values $\theta^{(i)}$ (i.e. the modules and phases) of the equivalent excitation systems applied to the first node that best fits the experimental data $\boldsymbol{\Xi}$, which is of order $\left(2l\, n_p \times 1\right)$, has to be estimated. Under a statistical point of view, a linear regression model is used, where $\boldsymbol{\theta}$ is the parameter vector to be estimated and $\mathbf{e}$ the error vector:

$$\boldsymbol{\Xi} = [\mathbf{Y}_{(1,\ldots,1)}]\boldsymbol{\theta} + \mathbf{e} = [\mathbf{Y}_{(1,\ldots,1)}]\begin{Bmatrix} \theta^{(1)} \\ \vdots \\ \theta^{(m)} \end{Bmatrix} + \mathbf{e} \tag{12}$$

Note that eq. (12) indicates a linear system also under a mechanical point of view, since the measured vibrations are caused by the superposition of the effects of all the excitation systems applied. The fitting of the regression model, i.e. the minimization of the error, can be done with different approaches.

2.1 Least squares estimate

The traditional approach is the least squares estimate (LS), since the number of the unknown (the modules and the phases of the equivalent excitations) is less than the equations. In fact data are corresponding to several rotating speeds and each of the sets is composed by several measuring planes, while the number of the faults in practical rotor dynamic applications is one or two; the occurrence of more than two simultaneous faults is an improbable event. The objective function to be minimized is:

$$\min \sum_{i=1}^{2ln_p} \left(e_i\right)^2 \leftrightarrow \min \sum_{i=1}^{2ln_p} \left(\Xi_i - [\mathbf{Y}_{(1,\ldots,1)_i}]\boldsymbol{\theta}\right)^2 \tag{13}$$

where $[\mathbf{Y}_{(1,\ldots,1)_i}]$ indicates the i-th row of $[\mathbf{Y}_{(1,\ldots,1)}]$. By skipping well-known mathematical derivations, the general solution of eq. (13) is obtained by means of the Moore-Penrose's inverse calculation:

$$\hat{\boldsymbol{\theta}}_{(1,\ldots,1)} = \left(\left[\mathbf{Y}_{(1,\ldots,1)}\right]^{\mathrm{T}}\left[\mathbf{Y}_{(1,\ldots,1)}\right]\right)^{-1}\left[\mathbf{Y}_{(1,\ldots,1)}\right]^{\mathrm{T}}\boldsymbol{\Xi} \tag{14}$$

The modules and the phases of the complex values in the m rows of $\hat{\boldsymbol{\theta}}_{(1,\ldots,1)}$ are the identified faults in the first rotor node. Finally the *relative residual* between the experimental data and the system response due to the identified faults in the first rotor node is determined, first by obtaining the calculated response due to the identified faults in the first node:

$$\hat{\boldsymbol{\Xi}}_{(1,\ldots,1)} = \left[\mathbf{Y}_{(1,\ldots,1)}\right]\hat{\boldsymbol{\theta}}_{(1,\ldots,1)} \tag{15}$$

then calculating the difference with the experimental data and normalizing it:

$$\hat{\delta}_{r_{(1,\ldots,1)}} = \left(\frac{\left[\boldsymbol{\Xi} - \hat{\boldsymbol{\Xi}}_{(1,\ldots,1)}\right]^{*\mathrm{T}}\left[\boldsymbol{\Xi} - \hat{\boldsymbol{\Xi}}_{(1,\ldots,1)}\right]}{\boldsymbol{\Xi}^{*\mathrm{T}}\boldsymbol{\Xi}}\right)^{1/2} \tag{16}$$

The procedure is subsequently iterated for all the permutations ${}_{n_r}P_m$ of the fault number and rotor nodes. If one fault only is considered (the system becomes a SIMO, single input multiple outputs), the set in $\square$ of relative residuals given by eq. (16) and ordered by the node number, is obtained:

$$\hat{\boldsymbol{\delta}}_r = \left(\hat{\delta}_{r_{(1)}}, \ldots, \hat{\delta}_{r_{(n_r)}}\right) \tag{17}$$

The s-th node location that corresponds to the minimum value of eq. (17) indicates the most probable location of the fault, the estimation of which is given by the corresponding value of eq. (14). If m faults are taken into account, all the permutations of the faults and the nodes have to be considered and the set of the relative residuals is in $\square^m$ space. The minimum of the set indicates in each one of the m dimensions the

location of the corresponding fault and their estimation is given by the corresponding value of the m rows eq. (14). The closer to zero the minimum value of eq. (17) is, the better the estimation of the faults is.

Anyhow, it is well known that LS is not a robust estimate (see [1][14][24] for a wide discussion about the concept of robustness in estimate) and this is shown also analytically in appendix. The presence of noise, of gross or systematic errors in the measurements can greatly reduce the accuracy of the identification. Some different methods are available to increase the robustness of LS [8][16], the simplest of which is the use of weighted least squares (WLS). WLS has given satisfactory results when applied to real rotating machines [2][7], but the selection of the weight should be made carefully and some skills are required.

2.2 Robust identification using M-estimate

The method presented in the paper is instead based on the use of M-estimate and allows selecting automatically the weights. At the authors' best knowledge it has never been applied to fault identification in rotor-dynamics and probably to mechanical systems in general. It requires two nested loops, so it requires longer calculation time, but greatly increases the robustness and therefore the accuracy of the obtained results. The external loop is relative to the localization of the fault and it is equal to that of the LS method. Therefore let's consider again to locate all the m equivalent exciting systems in the first node.

The idea is to obtain a robust estimate, by replacing the objective function of eq. (13) with another function ρ of the errors, the analytic expression of which will be introduced afterwards. The new function to be minimized is:

$$\min \sum_{i=1}^{2ln_p} \rho\left(e_i\right) \leftrightarrow \min \sum_{i=1}^{2ln_p} \rho\left(\Xi_i - [\mathbf{Y}_{(1,\ldots,1)_i}]\boldsymbol{\theta}\right) \tag{18}$$

To obtain the minimum, eq. (18) is derived with respect to e_i and put equal to zero. The *M-estimator* of $\boldsymbol{\theta}$ based on function $\rho(\mathbf{e})$ is the vector $\widehat{\boldsymbol{\theta}}$ solution of the m equations:

$$\sum_{i=1}^{2ln_p} \psi(e_i) \frac{\partial e_i}{\partial \theta^{(j)}} = 0 \quad \text{for} \quad j = 1,\ldots,m \tag{19}$$

where the derivate:

$$\psi(e_i) = \frac{\mathrm{d}\,\rho(e_i)}{\mathrm{d}\,e_i} \tag{20}$$

is proportional to the *influence function* [13][29] of the estimator and allows the analytical evaluation of its robustness. If the estimator is robust, the influence function is bounded and the influence of one single observation is insufficient to cause a significant error in the estimate. For the LS, the influence function is linear in Ξ_i (see eq. (13)) and therefore is not bounded. Further details are reported in appendix. Now, a *weight function* is defined as:

$$w(e_i) = \frac{\psi(e_i)}{e_i} \tag{21}$$

so that eq. (21) is rewritten as:

$$\sum_{i=1}^{2ln_p} w(e_i)\, e_i \frac{\partial e_i}{\partial \theta^{(j)}} = 0 \quad \text{for} \quad j = 1,\ldots,m \tag{22}$$

If the weights $w(e_i)$ are constant, the equation system in eq. (22) corresponds to that obtained to solve the problem:

$$\min \sum_{i=1}^{2ln_p} w(e_i) e_i^2 \tag{23}$$

which is actually a weighted least squares WLS with weights $w(e_i)$. Anyhow, actually the weights depend on the errors, the errors depend on the estimated excitations and the estimated excitations depend on the weights. To solve this vicious circle and justify the assumption of constant weights in the passage from eq. (22) to eq. (23), the second and inner loop is introduced by means of the use of an iterative solution, called *iterated re-weighted least squares* (IRLS) [9]. This way the weights are considered constant in each iteration:

1. The initial estimate of the amplitudes and phases of the excitation systems is selected using the results of least squares estimate, thus is that of eq. (14).
2. At each iteration t, the errors $e_i^{(t-1)}$ and the associated weights $w_i^{(t-1)}$ are calculated from the previous iteration.
3. The new weighted least squares estimate at iteration t is:

$$\hat{\boldsymbol{\theta}}_{(1,\ldots,1)}^{(t)} = \left(\left[\mathbf{Y}_{(1,\ldots,1)} \right]^{\mathrm{T}} \left[\mathbf{W}^{(t-1)} \right] \left[\mathbf{Y}_{(1,\ldots,1)} \right] \right)^{-1} \left[\mathbf{Y}_{(1,\ldots,1)} \right]^{\mathrm{T}} \left[\mathbf{W}^{(t-1)} \right] \boldsymbol{\Xi} \tag{24}$$

where:

$$\left[\mathbf{W}^{(t-1)} \right] = \mathrm{diag} \left[w_i^{(t-1)} \right] \tag{25}$$

Steps 2 and 3 are iterated until convergence of the values of $\hat{\boldsymbol{\theta}}_{(1,\ldots,1)}$ is achieved upon a stated criterion. The inner loop is then ended and the relative residual for the first rotor node, obtained with M-estimate, is calculated similarly to that in case of least squares:

$$\hat{\boldsymbol{\Xi}}_{(1,\ldots,1)} = \left[\mathbf{Y}_{(1,\ldots,1)} \right] \hat{\boldsymbol{\theta}}_{(1,\ldots,1)} \tag{26}$$

and:

$$\hat{\delta}_{r_{(1,\ldots,1)}} = \left(\frac{\left[\boldsymbol{\Xi} - \hat{\boldsymbol{\Xi}}_{(1,\ldots,1)} \right]^{*\mathrm{T}} \left[\boldsymbol{\Xi} - \hat{\boldsymbol{\Xi}}_{(1,\ldots,1)} \right]}{\boldsymbol{\Xi}^{*\mathrm{T}} \boldsymbol{\Xi}} \right)^{1/2} \tag{27}$$

The procedure then follows with the external loop and is iterated as in the LS case, so that the set of $\hat{\boldsymbol{\delta}}_r$ in the $\mathbb{R}^m$ space is built up. Once again, the minimum value of $\hat{\boldsymbol{\delta}}_r$ indicates along the m dimensions the most probable location of the faults, the estimation of which is given by the corresponding values of $\hat{\boldsymbol{\theta}}_{(s)}$.

The ρ functions have generically to posses to some properties, listed in [10], and their performances can be also outlined analytically. Several ρ functions have been proposed in statistical literature and a pretty complete survey is reported in [29]. Some tests on different ρ functions have been performed by the authors [5] to select the most suitable for mechanical application and Huber's function presented satisfactory performances.

The aim of Huber's estimator is to find the simplest imaginable function that is consistent with the conditions of robustness. Huber introduced it [8][14][16] to give the minmax solution to eq. (19) for normal distributions affected by noise, under the hypothesis of known scale parameter $\hat{\sigma}$ and then it was extended to general

distributions. He started from the maximum likelihood estimator (MLE) and reduced its sensitivity to the outliers. For a data sample with distribution density f, the MLE maximizes:

$$\sum \log f(x-\theta) \tag{28}$$

It can be defined by considering that, if the sample distribution is unknown, the most reasonable assumption is to suppose the symmetry:

$$f(x-\theta) \approx f(\theta-x) \tag{29}$$

The Taylor's expansion in proximity of the centre of the symmetric distribution is:

$$f(x) \approx f(\theta) - (x-\theta)^2/2 \tag{30}$$

In the proximity of the centre can be written that:

$$\log f(x-\theta) \approx \frac{(x-\theta)^2}{2} \tag{31}$$

plus a constant. Therefore the parabola:

$$\rho(x-\theta) = \frac{(x-\theta)^2}{2} \tag{32}$$

is the optimal choice in the proximities of the centre. This notwithstanding eq. (32) coincides to the least squares, which are not robust. A possibility is to limit the influence function if the residue exceeds a certain value, called *tuning parameter* c [9]. The resulting ρ, ψ and w functions are:

$$\rho(e_i) = \begin{cases} \frac{e_i^2}{2} & \text{if } |e_i| \le c \\ c\left(|e_i| - \frac{c}{2}\right) & \text{if } |e_i| > c \end{cases}; \quad \psi(e_i) = \begin{cases} e_i & \text{if } |e_i| \le c \\ c\,\mathrm{sgn}(e_i) & \text{if } |e_i| > c \end{cases}; \quad w(e_i) = \begin{cases} 1 & \text{if } |e_i| \le c \\ \frac{c}{|e_i|} & \text{if } |e_i| > c \end{cases} \tag{33}$$

Therefore different estimators can be obtained depending on the value of the tuning parameter. Since this estimator has been developed originally for normal distributions, the optimal tuning parameter c is calculated in order to have the 95% of asymptotic efficiency with respect to a normal distribution and results $c = 1.3450\,\hat{\sigma}$, where $\hat{\sigma}$ is the scale parameter [25] of the error distribution. The selection of the scale parameter would worth a long discussion: M-estimators for simultaneous location and scale estimate have been proposed in literature starting from [14]. Nevertheless the application presented here is rather different because, contrarily to traditional statistical applications, the error distribution is a bivariate distribution (in general, being the measured vibrations complex numbers, $e_i \in \mathbb{C}$) and a robust bivariate scale parameter should be used. For sake of brevity, the authors introduce a proposal without discussing it that is based on the extension of the median absolute deviation (MAD) to the complex field using the Tukey's median instead of the conventional median. If $\mathbf{T}^*(\cdot)$ is the Tukey's median operator, the extension of the MAD is here defined as TMAD (Tukey's median absolute deviation):

$$\mathrm{TMAD}(\mathbf{e}) = \mathrm{Med}\left(\left|\mathbf{e} - \mathbf{T}^*(\mathbf{e})\right|\right) \tag{34}$$

Details on Tukey's median calculation are presented in [26][22].

3 EXPERIMENTAL RESULTS

The improvements in the accuracy obtained by using the M-estimate instead of the LS are presented by means of the identification of faults in two different rotating machines: the test-rig of Polytechnic of Milan (PdM) and a 125 MW gas turbo-generator of a power plant.

3.1 Increasing the fault identification accuracy in the PdM test-rig

The test rig, shown in figure 1 and figure 2, is composed of two rigidly coupled steel shafts, driven by a variable speed electric motor and supported by four elliptical shaped oil film bearings. Rotor train is long about two meters and has a mass of about 90 kg. The rotors have three critical speeds within the operating speed range of 0-6000 rpm. The model of the rotor has been tuned and the stiffness and damping coefficients of the bearings determined with accuracy, as described in [3].

Figure 1: PdM test-rig.

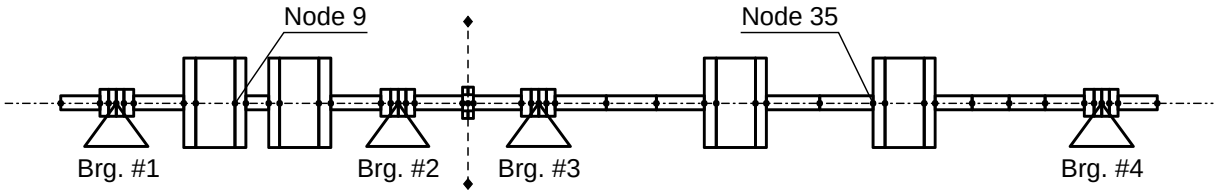

Figure 2: Rotor model of PdM test-rig.

The rotor system is mounted upon a flexible steel foundation that has several natural frequencies in the operating speed range of the rotor. In this case the foundation has been modelled by means of a modal representation. Two proximity probes in each bearing measure the relative shaft displacements; two accelerometers on each bearing housing measure its vibrations, and two force sensors on each bearing housing measure the forces which are transmitted to the foundation. The absolute vibration of the shaft is calculated by adding the relative displacement measured by the proximity probes to the absolute bearing housing displacement, which is obtained integrating twice the acceleration measured by the accelerometers. The force measurements were not used in this case. One run-down test was performed in order to store a reference vibration data.

3.1.1 Unbalance on the long shaft

The first test-case is relative to the application of a known unbalance on the long shaft on the fourth inertia disk. The corresponding node in the finite beam model is 35, the unbalance amplitude is 3.6e–4 kgm with phase –90°. The vibration measurements are taken again during one run-down and the additional vibrations are finally obtained by subtracting the reference vibrations. The speed range is between 544 and 2696 rpm.

The fault identification is performed by using both the LS-estimate with all the available data and the M-estimate with the Huber's function. The algorithms are simplified with respect to the general cases presented in section 2, since one fault only is identified (the system is SIMO). Since the estimated values are complex, the IRLS algorithm is repeated until the maximum relative difference between the real and the imaginary parts in the last iteration and those of the previous iteration is less than 1e–4. Note that the convergence criterion is very restrictive and in any case the inner loops are stopped after 100 iterations.

The results are summarized in table 1 that shows that the LS-estimate does not exactly identify the position of the unbalance, under-estimates the module and over-estimates the phase. Anyhow the results are not completely bad under an engineering point of view. This is due to the overall quality of the model that is tuned and to the accurate measurements. The M-estimate gives instead outstanding results, not only identifying exactly the position of the unbalance, but also with negligible errors on the module and the phase. The quality of the identification of the M-estimate is also shown by the value of the relative residual that is lower than that of LS-estimate, even if the minima are in different nodes, as also shown in figure 3, where the $\hat{\boldsymbol{\delta}}_r$ and $\bar{\hat{\boldsymbol{\delta}}}_r$ successions are plotted.

Table 1: Identification results of unbalance on the long shaft of PdM test-rig.

	Node	$\Delta l\,[m]$	Module [kgm]	Δmr [kgm]	Phase	$\Delta\varphi$	Rel. residual
Actual	35		3.60 e–4		–90°		
LS-estimate	36	0.02 (1.03%)	3.17 e–4	–0.47e–4 (–13.06%)	–80.42°	9.58°	0.521
M-estimate	35	0.00 (0.00%)	3.62 e–4	0.02e–4 (0.56%)	–89.38°	0.62°	0.334

It is also interesting to check the convergence of the equivalent exciting system parameters during the IRLS loop. In particular, in correspondence of the node 35, where the M-estimate locates the fault that is the actual location too, the estimate of the parameter as a function of the number of iterations is shown in figure 4. Note that the convergence is reached at the 93rd iteration and that the estimate in the 1st iteration is that of LS, which differs from that of table 1, since $\hat{\boldsymbol{\delta}}_r$ has its minimum in node 36. If the stop criterion of the IRLS algorithm were relaxed, convergence would be reached with much less iterations.

The last analysis presented for this case study is the comparison between the experimental measurements and the system simulated response by applying the fault parameters identified with the two estimates (figure 5-figure 14). Figure 5 shows the comparison for the vertical direction of brg. #1 and the weights $w_i^{(t)}$ of the last step of the IRLS loop. The simulated responses obtained solving eq. (1) directly with the two fault parameter estimate of table 1, show a general good agreement in both LS and M-estimate case, being the M-estimate better. Moreover it is possible to observe that, when the simulated response of M-estimate tends to shift from the experimental

response in amplitude or phase, the algorithm assigns weights $w_i^{(t)}$ generally less than 1 by itself. This fact is manifest also for the other bearings and particularly evident for instance in figure 7, where the sets of measurements weighted correspond to rather contiguous values of the rotating speed that are grey shaded. In the range 899-950 rpm the fit is not good for the phase, in 1000-1178 rpm the fit is bad for the amplitude and partially for the phase, in 1729-2035 rpm, 2156-2598 rpm and 2655-2678 rpm is not good for the amplitude.

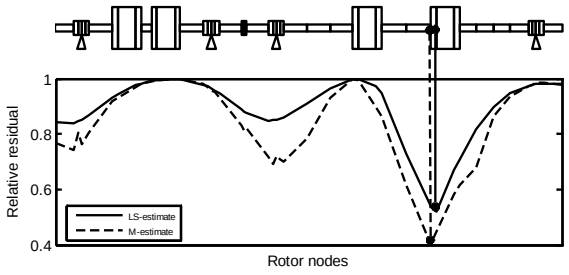

Figure 3: Relative residuals along the test rig for the first test-case.

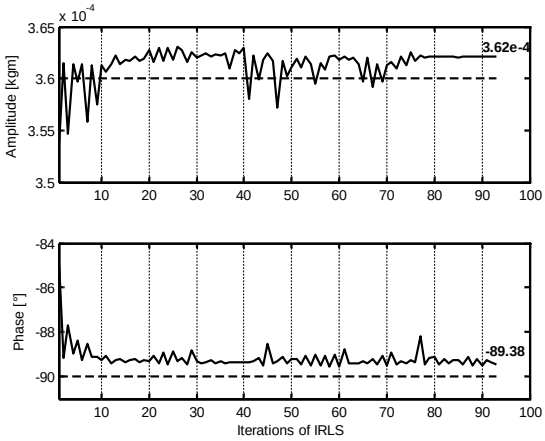

Figure 4: Convergence of estimated parameters during IRLS iterations in node 35.

Note that each weight w_i is assigned to a certain measure of a certain output among the multiple outputs of the system. This is a very special characteristic of the M-estimate, which is not obviously available in the standard LS and in any case practically impossible to achieve automatically in general WLS, where measures are often grouped and weighted per speed ranges and per output channels by expert's selection.

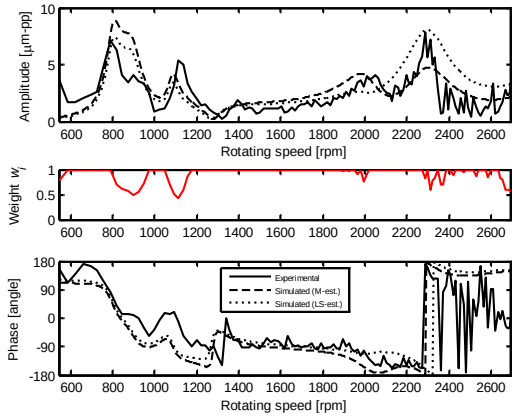

Figure 5: Experimental, simulated vibrations with LS and M-estimate and vibrations weights in last step of ILRS loop, brg. #1, vertical direction.

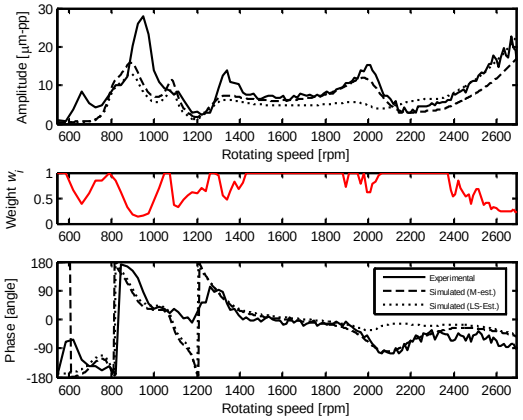

Figure 6: Experimental, simulated vibrations with LS and M-estimate and vibrations weights in last step of ILRS loop, brg. #1, horizontal direction.

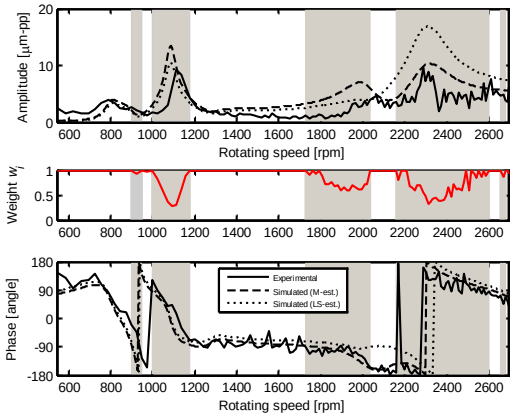

Figure 7: Experimental, simulated vibrations with LS and M-estimate and vibrations weights in last step of ILRS loop, brg. #2, vertical direction.

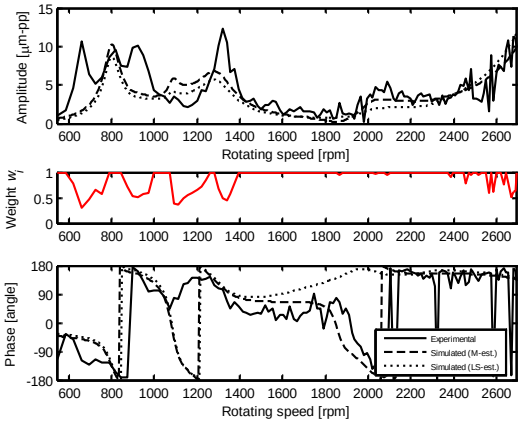

Figure 8: Experimental, simulated vibrations with LS and M-estimate and vibrations weights in last step of ILRS loop, brg. #2, horizontal direction.

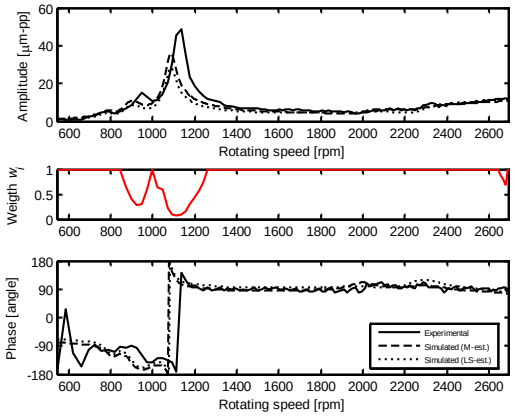

Figure 9: Experimental, simulated vibrations with LS and M-estimate and vibrations weights in last step of ILRS loop, brg. #3, vertical direction.

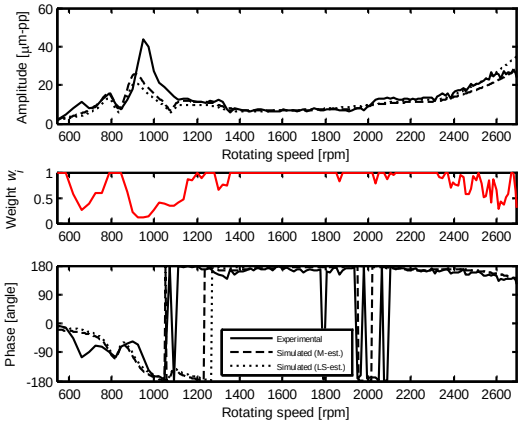

Figure 10: Experimental, simulated vibrations with LS and M-estimate and vibrations weights in last step of ILRS loop, brg. #3, horizontal direction.

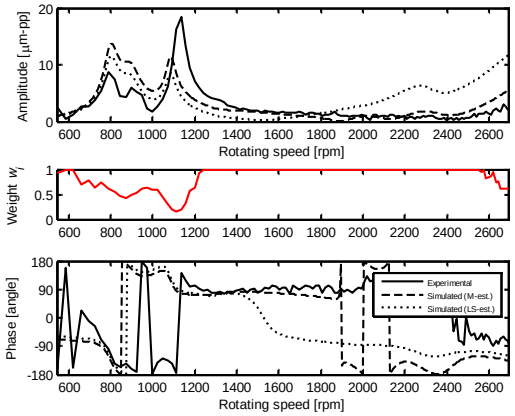

Figure 11: Experimental, simulated vibrations with LS and M-estimate and vibrations weights in last step of ILRS loop, brg. #4, vertical direction.

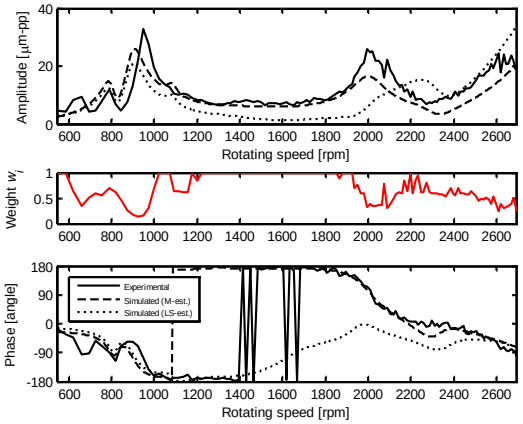

Figure 12: Experimental, simulated vibrations with LS and M-estimate and vibrations weights in last step of ILRS loop, brg. #4, horizontal direction.

3.1.2 Unbalance on the short shaft

The second test-case on PdM test-rig is relative to the application of one known unbalance on the short shaft on the first inertia disk. The corresponding node in the finite beam model is 9, the amplitude and the phase are the same of the previous case, i.e. 3.6e–4 kgm and –90°. Additional vibrations are obtained with respect to the same reference vibrations in the speed range 544-2696 rpm. The results are summarized in table 2. Again the LS-estimate does not locate exactly the position of the fault, while M-estimate does. The results of amplitude and phase are generally worse than those of table 1, even if M-estimate is always more accurate. For sake of conciseness, the comparison between the experimental measurements and the simulated results with the identified fault parameters is shown in figure 13 and figure 14 for brg. #1 only. The comments that can be drawn are similar to those of the previous case, also for the results in the bearings not shown.

Table 2: Identification results of unbalance on the short shaft of PdM test-rig.

	Node	$\Delta l\,[m]$	Module [kgm]	Δmr [kgm]	Phase	$\Delta\varphi$	Rel. residual
Actual	9		3.60 e–4		–90°		
LS-estimate	7	–0.09 (–4.61%)	4.44 e–4	0.84e–4 (23.33%)	–95.16°	–5.16°	0.624
M-estimate	9	0.00 (0.00%)	3.98 e–4	0.38e–4 (10.55%)	–91.50°	–1.50°	0.506

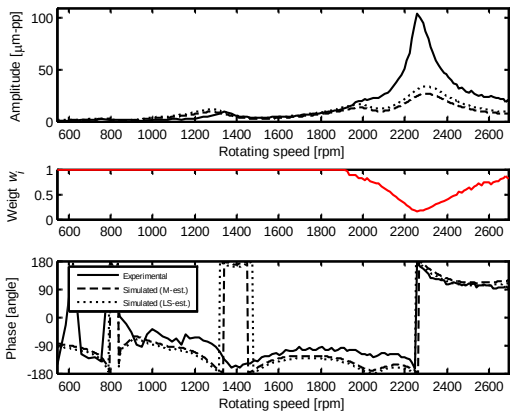

Figure 13: Experimental, simulated vibrations with LS and M-estimate and vibrations weights in last step of ILRS loop, brg. #1, vertical direction.

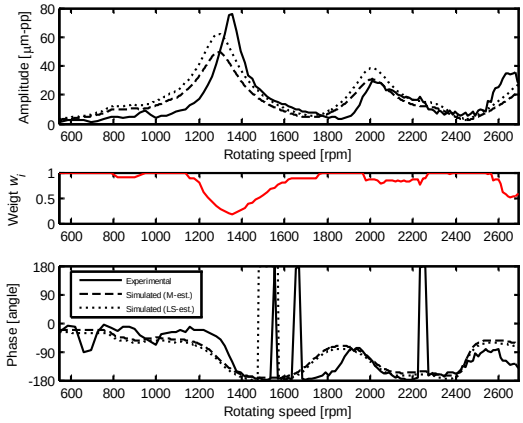

Figure 14: Experimental, simulated vibrations with LS and M-estimate and vibrations weights in last step of ILRS loop, brg. #1, horizontal direction.

3.1.3 Twin unbalances

The third test-case presented is actually a MIMO: two known unbalance are applied on both shafts of PdM test-rig. The balancing planed considered are those of the previous cases, so that he corresponding nodes in the finite beam model are 9 (unbalance on the short shaft) and 35 (unbalance on the short shaft). Also the amplitude and the phase of both unbalances are the same of the previous case, i.e. 3.6e–4 kgm and –90°. Using the same stored reference vibrations, the additional vibrations are obtained in the speed range 504-3001 rpm. Being two unbalances simultaneously identified, the relative residuals are calculated for the permutations ${}_{n_r}P_2$ and their set

is in $\square^2$. Since the two faults are of the same kind, the residual surface is symmetric and has therefore two minima.

Anyway, it is not easy to immediately identify the minimum in the surface of $\hat{\boldsymbol{\delta}}_r$ and $\widehat{\boldsymbol{\delta}}_r$, therefore a different representation, called *residual map* is used, in which colour code represent the value of the residual and vertical and horizontal axis correspond to the rotor nodes. Using the residual map, the residuals are plotted in figure 17 for the LS-estimate and in figure 18 for the M-estimate, the grey-scale is adopted only for residuals minor than 0.6 in order to make easy the identification of the faults. The two darkest areas indicate the position of the two faults. It is possible to see that the M-estimate locates correctly the fault position, whilst LS-estimate does not. The complete results are summarized in table 3. Also in this case, the M-estimate achieve greater accuracy than LS-estimate, not only with regards to the fault positions, but also to amplitudes and phases of the unbalances.

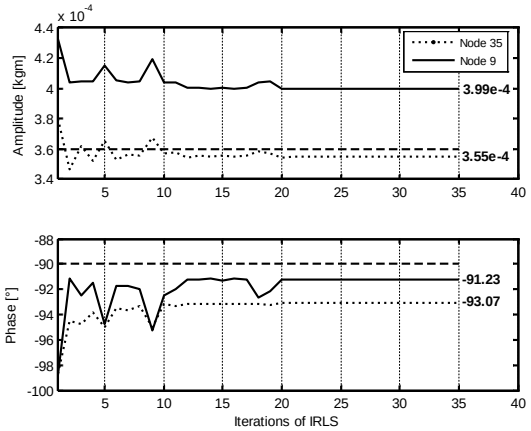

Figure 15: Convergence of estimated parameters during IRLS iterations when the unbalances are located in nodes 9 and 35.

Table 3: Identification results of two simultaneous unbalance on PdM test-rig.

	Nodes	$\Delta l\,[m]$	Module [kgm]	Δmr [kgm]	Phase	$\Delta\varphi$	Rel. residual
Actual	9		3.60 e–4		–90°		
	35		3.60 e–4		–90°		
LS-estimate	8	–0.07 (–3.59%)	4.22 e–4	0.62e–4 (17.22%)	–93.21°	–3.21°	0.578
	36	0.02 (1.03%)	3.82 e–4	0.22e–4 (6.11%)	–102.52°	–12.52°	
M-estimate	9	0.00 (0.00%)	3.99 e–4	0.39e–4 (10.83%)	–91.23°	–1.23°	0.415
	35	0.00 (0.00%)	3.55 e–4	–0.05e–4 (–1.39%)	–93.07°	–3.07°	

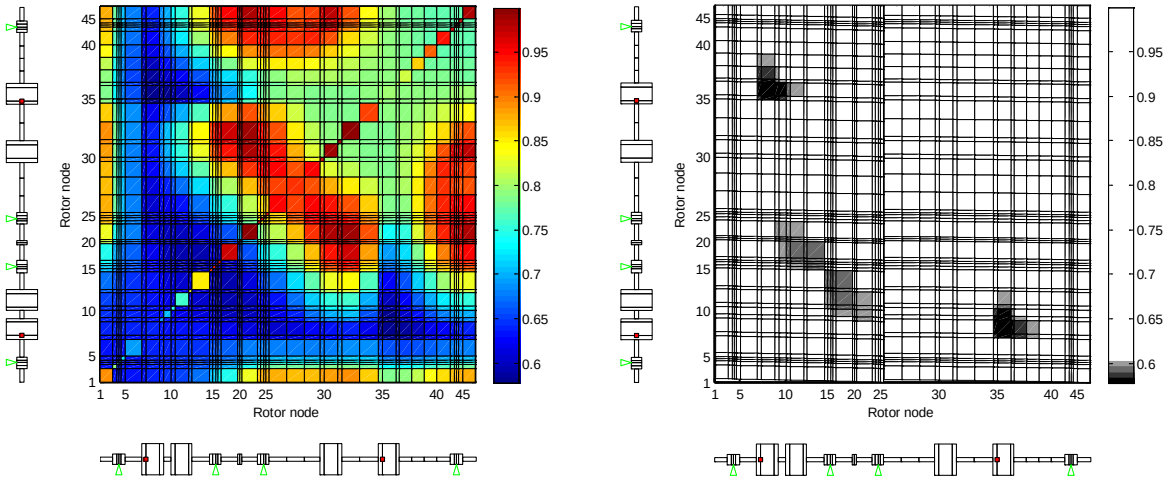

Figure 16: Residual map for the LS-estimate (the grey-scale on the left has cut-off at 0.6 to highlight the minima position).

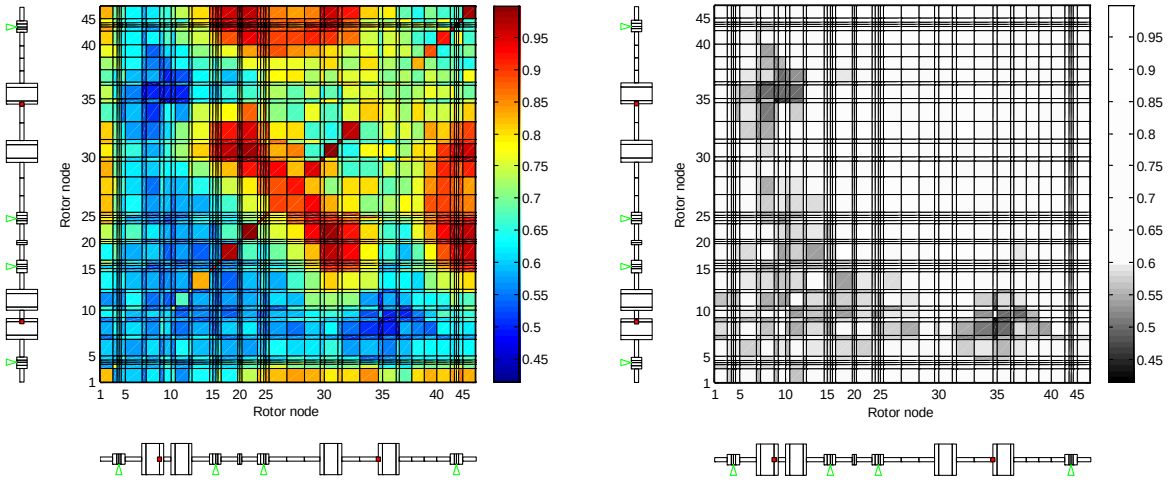

Figure 17: Residual map for the M-estimate (the grey-scale on the left has cut-off at 0.6 to highlight the minima position).

It is also interesting to note that, even if the stop condition of the IRLS algorithm is quite restricted, the convergence of the estimated values of the two faults in correspondence of the minimum value of the $\widehat{\boldsymbol{\delta}}_r$ occurs before than the maximum allowed number of iterations (see figure 16). Anyway, on the basis of the preliminary studies presented in [5], it is not possible to asses that the convergence of a MIMO problem, like this case, should be faster than a SIMO, like that of section 3.1.1.

Finally the comparison between the experimental measurements and the simulated results with the identified fault parameters is shown in figure 19 to figure 22 for brgs. #1 and #3 only. The comments that can be drawn are similar to those of the previous cases, also for the results in the bearings not shown.

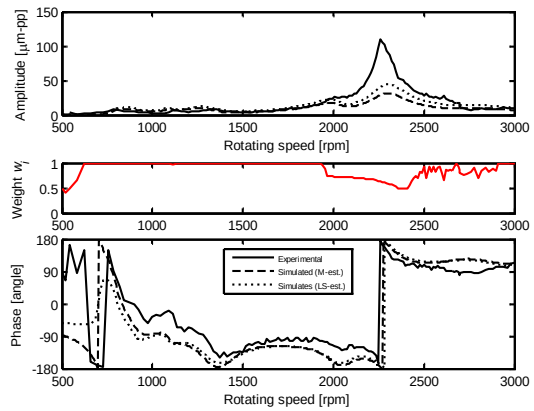

Figure 18: Experimental, simulated vibrations with LS and M-estimate and vibrations weights in last step of ILRS loop, brg. #1, vertical direction.

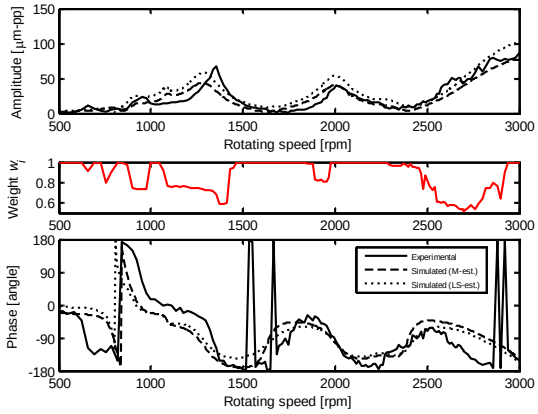

Figure 19: Experimental, simulated vibrations with LS and M-estimate and vibrations weights in last step of ILRS loop, brg. #1, horizontal direction.

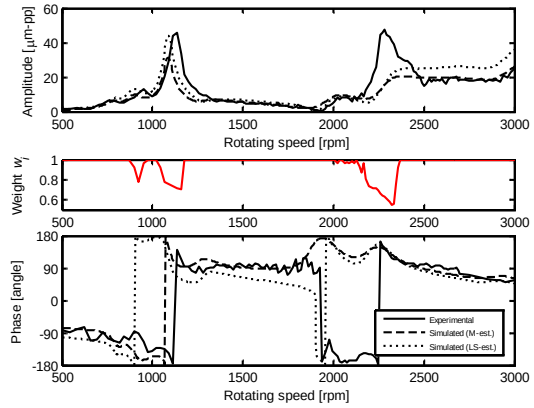

Figure 20: Experimental, simulated vibrations with LS and M-estimate and vibrations weights in last step of ILRS loop, brg. #3, vertical direction.

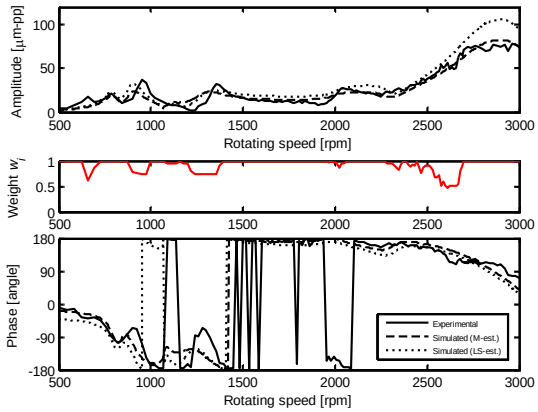

Figure 21: Experimental, simulated vibrations with LS and M-estimate and vibrations weights in last step of ILRS loop, brg. #3, horizontal direction.

3.2 Increasing the fault identification accuracy in a gas turbo-generator

Since the aim of the proposed M-estimate method applied to rotor-dynamics problems is to increase accuracy in the identification of faults, being contemporaneously robust, the second example shown is related to a real machine, a 125 MW gas turbo-generator (figure 23), employed in combined cycle plants, operating at rated speed of 3000 rpm, the model of which is not tuned. The rotor model and the layout of the rotor train are shown in figure 24, in which the three shafts that compose the rotor train are clearly recognizable. From left to right they are:

- the turbine, with the exhaust on the left side, of approximate length of 9.539 m and mass of 53434 kg;
- the connecting shaft, of approximate length of 1.721 m and mass of 2423 kg;
- the generator, of approximate length of 9.083 m and mass of 26870 kg.

The overall length is therefore 20.343 m and the mass 82727 kg. Four oil film bearings support the rotor train, those on the turbine are of tilting pad type, while those of the generator are of partial arc type. Measuring planes of the vibrations are corresponding to the bearings.

Figure 22: Close up of the compressor and turbine of the considered gas turbo-generator.

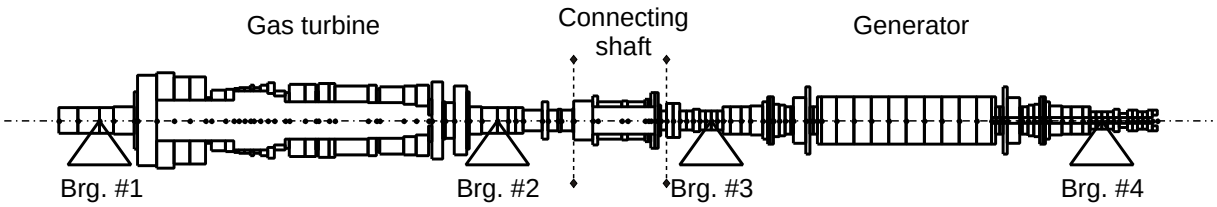

Figure 23: Rotor model of a gas turbo-generator.

The rotor model shown in figure 24 has 125 nodes. The available experimental results are related to run-downs of some balancing operations, the details of which are described in [6]. In that paper it was shown that the fault identification using WLS gave satisfactory results with an accurate expert's selection of the data, based on the consideration that the model is adequate in a specific speed range, but the accuracy of the identification of the fault parameters was not high, due also to the lack of global tuning of the model. In this paper four different WLS criteria are used, reflecting expert's selection based on both measuring planes and speed range. The sets of weights are:

- $\mathbf{V}_1$: machine model is given by the manufacturer and it is believed to be adequate in the range 2500-3000 rpm. This set of weights considers only the data in this speed range;
- $\mathbf{V}_2$: this set considers the data of all the available speed transient;
- $\mathbf{P}_1$: since higher vibrations are on the gas turbine, this set assigns unitary weight to measuring planes of the turbine and 0.5 to those of the generator;
- $\mathbf{P}_2$: all measuring planes have unitary weights.

The WLS combination is reported in

Table 4: WLS combination.

	$\mathbf{P}_1$	$\mathbf{P}_2$
$\mathbf{V}_1$	WLS_1 : data in the speed range 2500-3000 rpm only, measuring planes of turbine have weight equal to 1, those of generator equal to 0.5	WLS_2 : data in the speed range 2500-3000 rpm, all measuring planes have weight equal to 1
$\mathbf{V}_2$	WLS_3 : data of all the speed transient, measuring planes of turbine have weight equal to 1, those of generator equal to 0.5	LS-estimate: data of all the speed transient, all measuring planes have weight equal to 1. this combination is really LS-estimate

Finally, the M-estimate is applied to show that also in presence of these disadvantageous conditions, i.e. model not tuned up, it is possible to increase the accuracy, without expert's skill. Two test-cases are presented.

3.2.1 First test-case

The first test-case is relative to one balancing weight of 0.373 kgm with phase 157.5° applied to the balancing plane immediately close to turbine exhaust, which corresponds to node 6 of the model. Additional vibrations are available in the speed range 11-3000 rpm. The available measurements at very low rotating speeds should be discarded, since the corresponding linearized stiffness and damping coefficients of the bearings are not reliable at all, but it has been deliberately decided to include them in order to represent a "blind strategy".

The results are summarized in table 5. WLS and LS-estimate are not very different, therefore only LS-estimate results are used in the following figures. The M-estimate localizes exactly the fault (figure 25) and improves also the accuracy of the unbalance module and phase identification. The better quality of the identification of the M-estimate is also shown by the value of the relative residual that is lower than that of WLS and LS-estimate, even if the minima are in different nodes, as also shown in figure 26, where $\hat{\boldsymbol{\delta}}_r$ and $\bar{\boldsymbol{\delta}}_r$ successions only are plotted for clarity.

Table 5: Identification results of unbalance on balancing plane close to the exhaust of the gas turbine.

	Node	$\Delta l\,[m]$	Module [kgm]	Δmr [kgm]	Phase	$\Delta\varphi$	Rel. residual
Actual	6		0.373		157.50°		
WLS_1	4	–0.442 (–2.18%)	0.631	0.258 (69.17%)	118.35°	–39.15°	0.633
WLS_2	4	–0.442 (–2.18%)	0.575	0.202 (54.16%)	121.70°	–35.80	0.657
WLS_3	4	–0.442 (–2.18%)	0.603	0.230 (61.66%)	123.41°	–34.09	0.627
LS-estimate	4	–0.442 (–2.18%)	0.586	0.213 (57.10%)	122.70°	–34.80°	0.669
M-estimate	6	0.00 (0.00%)	0.458	0.085 (22.79%)	134.87°	–22.63°	0.603

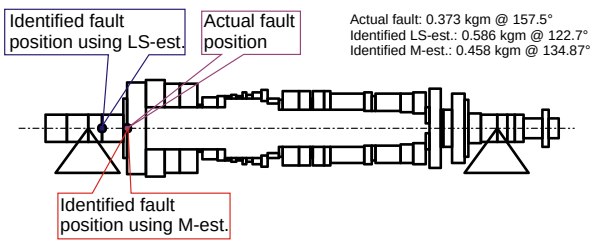

Figure 24: Location of the identified faults (generator and connecting shaft omitted for clarity).

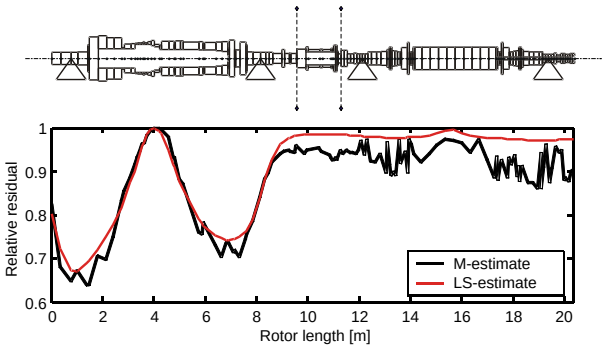

Figure 25: Relative residuals along the rotor.

Anyway, some inaccuracies are still present when M-estimate is used. The reason is rather evident from figure 27 and figure 28 that show the comparison between the experimental measurements and the simulated results with the identified fault parameters for brg. #2. Few of the values $w_i^{(t)}$ are equal to 1 and this indicates poor quality of the model used to fit the data. In fact the model is not able to reproduce the resonance at about 850 rpm (due to the supporting structure). Similar considerations can be made also analyzing the comparisons in the other bearings.

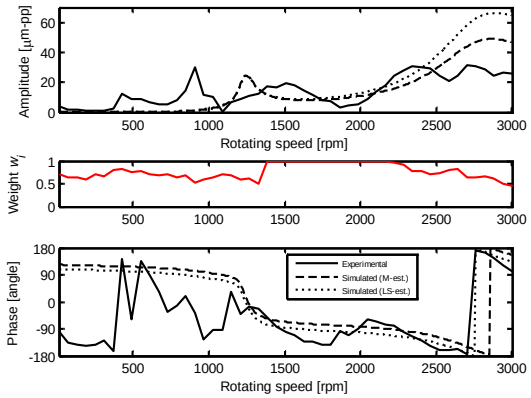

Figure 26: Experimental, simulated vibrations with LS and M-estimate and vibrations weights in last step of ILRS loop, brg. #2, vertical direction.

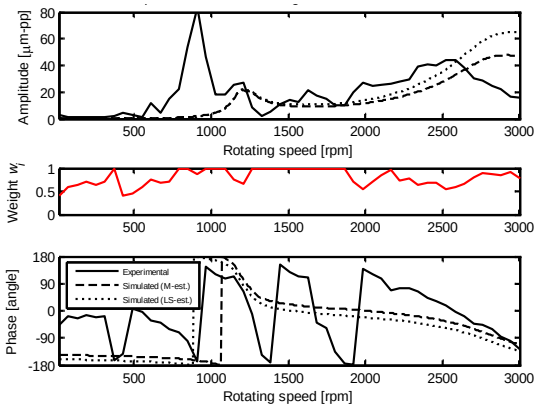

Figure 27: Experimental, simulated vibrations with LS and M-estimate and vibrations weights in last step of ILRS loop, brg. #2, horizontal direction.

3.2.2 Second test case

The second test-case is relative to one balancing of 0.270 kgm with phase 52° on the balancing plane immediately close to turbine intake, which corresponds to node 39 of the model. Additional vibrations are available in the speed range 3-3000 rpm. The results are summarized in table 5. In this case, neither M-estimate can locate exactly the position of the fault, even if the error practically negligible (figure 29). WLS_1 gives a very bad result because fault position actually excites also vibrations in bearing #3, the measurements of which are weighted 0.5. Similarly to the previous case, the accuracy of identified parameters has increased by applying M-estimate and the results can be deemed satisfactory under an engineering point of view, but better tuning of the model would have improved them, as could be shown by means of the comparison between experimental results and simulated response and of the analysis of the weights. Since these diagrams are conceptually similar to those of the previous case, they are not reported for brevity.

Table 6: Identification results of unbalance on balancing plane close to the intake of the gas turbine.

	Node	$\Delta l\,[m]$	Module [kgm]	Δmr [kgm]	Phase	$\Delta\varphi$	Rel. residual
Actual	39		0.270		52°		
WLS_1	16	4.285 (21.1%)	0.487	0.217 (80.37%)	113.78°	61.78°	0.930
WLS_2	41	0.440 (2.17%)	0.172	–0.098 (–36.30%)	63.0°	11.0°	0.878
WLS_3	42	0.622 (3.06%)	0.182	–0.088 (–32.59%)	65.21°	13.21°	0.922
LS-estimate	41	0.440 (2.17%)	0.168	–0.102 (–37.78%)	62.60°	10.60°	0.928
M-estimate	40	0.050 (0.29%)	0.215	–0.055 (–20.37%)	51.68°	–0.32°	0.858

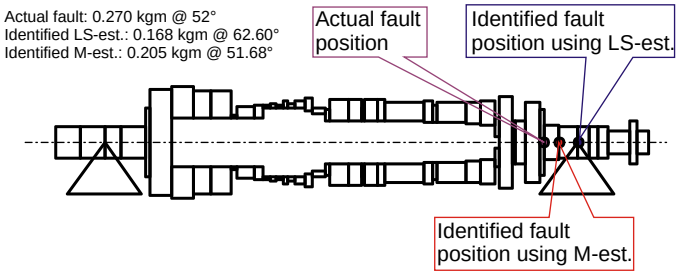

Figure 28: Location of the identified faults (generator and connecting shaft omitted for clarity).

4 CONCLUSION

The M-estimate technique applied to faults identification in rotor dynamics has been presented in the paper. This technique represents an interesting way to increase the robustness and the accuracy of the LS-estimate in the frequency domain. Since it allows defining automatically the weights to be assigned to each experimental data, without external actions, it makes the identification robust with respect to gross errors, outliers and model local inaccuracies. Moreover, it reduces the arbitrary intervention of the operator and allows accurate results also to no-expert users. The required algorithm has been described in detail and can be extended to every MIMO inverse problems.

The validation of the presented technique has been performed by means of identification of known faults, in this case unbalances, in a test-rig and in a real machine (a gas turbo-generator of a power plant). Experimental cases of both SIMO and MIMO systems are presented. In all the test-cases presented, the accuracy in the fault identification was better than that of LS-estimate, indicating the improvement in the robustness.

APPENDIX – INFLUENCE FUNCTION

The analytical tool that allows to evaluate the robustness of an estimator in presence of outliers and gross errors is the *influence function* introduced by Hampel [12][13]. In order to allow more intuitive interpretation of its definition (as suggested in [24]), it is introduced as the limit of the *sensitivity curve*, proposed by Tukey [17] to evaluate the stability of an estimator. Let $(X_1, X_2, \ldots, X_n)$ a random sample extracted from $X \sim F(x;\theta)$, i.e.

the actual sample distribution is F and depends from the parameter θ. The parameter θ is going to be estimated by means of the estimator $T_n = T(X_1, X_2, \ldots, X_n)$ that can be defined as follows. The empirical distribution function is:

$$F_n(u) = \frac{1}{n}\sum I\left(X_i \le u\right), \tag{35}$$

which attributes to every observation equal probability $1/n$. The operator $I(\cdot)$ indicates the number of i that satisfies the condition $\cdot$ inside the parentheses.

Obviously, the knowledge of the random sample or of the empirical distribution function is equivalent, because the random sample is immediately inferred from $F_n(x)$ and, vice versa, the sample is immediately inferred from the empirical distribution function because $F_n(x)$ introduces some jumps in correspondence of the sample values. This justifies denoting the estimator as a functional of the empirical distribution function: $T_n = T[F_n]$.

Now, if an arbitrary observation x is added to the random sample $(X_1, X_2, \ldots, X_n)$, a new sample $(X_1, X_2, \ldots, X_n, x)$ is obtained, the empirical distribution function of which is $F_{n+1}(u; x)$. It is easy to demonstrate that:

$$F_{n+1}(u; x) = \frac{1}{n+1}\sum_{i=1}^{n} I\left(X_i \le u\right) + \frac{1}{n+1} I\left(x \le u\right) = \frac{n}{n+1} F_n(u) + \frac{1}{n+1} I\left(x \le u\right). \tag{36}$$

If $\delta_x(u)$ indicates the distribution function of a random anomalous variable in x and $\varepsilon = \frac{1}{n+1}$, then:

$$F_{n+1}(u; x) = (1-\varepsilon)F_n(u) + \varepsilon\,\delta_x(u) = (1-\varepsilon)F_n + \varepsilon\,\delta_x. \tag{37}$$

Similarly, the estimator $T_n = T[F_n]$ defined on $(X_1, X_2, \ldots, X_n)$ becomes:

$$T_{n+1}(x) = T\left[F_{n+1}(u; x)\right] = T\left[(1-\varepsilon)F_n + \varepsilon\,\delta_x\right]. \tag{38}$$

when it shifts on the extended sample $(X_1, X_2, \ldots, X_n, x)$. The condition that makes T_n an acceptable estimate for θ is that the addition of an observation x to the random sample does not strongly modify its value. The most straightforward way to measure the effect of this addiction is to consider the difference between $T_{n+1}(x)$ and T_n and to compare it to the weight of the added observation (measured by ε), that obviously is inversely proportional to the sample number. This defines the *sensitivity curve* of the estimator T_n [17]:

$$SC_n(x, T) = \frac{T_{n+1}(x) - T_n}{\varepsilon} = \frac{T\left[(1-\varepsilon)F_n + \varepsilon\,\delta_x\right] - T[F_n]}{\varepsilon}. \tag{39}$$

The sensitivity curve can be studied as a function of x for an estimator T_n. If the observation x is far away from the majority of the data, the curve of sensitivity shows what happens to the estimator when this outlier is present in the sample. Therefore, it is necessary that $SC_n(x, T)$ is limited, so that the effect of an outlier to the estimator is always restricted within defined limits.

If $n \to \infty$, the Glivenko-Cantelli's theorem states that $F_n(x)$ converges uniformly and in distribution to $F(x)$. Moreover, for Fisher's consistent estimators $T[F_n] \to T[F] = \theta$ and $T[F_n]$ can be replaced asymptotically by $T[F]$. The *influence function* of the estimator T_n with respect to $F(x; \theta)$ is:

$$IF(x, T, F) = \lim_{\varepsilon \to 0} \frac{T\left[(1-\varepsilon)F + \varepsilon\,\delta_x\right] - T[F]}{\varepsilon} = \frac{\partial}{\partial \varepsilon} T[F]\bigg|_{\varepsilon = 0}. \tag{40}$$

The influence function shows the asymptotic variation of $T[F]$ due to an infinitesimal contamination of the distribution $F(x)$, related to the contamination entity. The influence function depends on x, as the sensitivity curve, but also on $F(x)$, that is on the parametric model supposed for the data. Therefore, it represents a parametric tool that can be used to verify the behaviour of an estimator in the cases in which the "actual" distribution is close to the hypothesized distribution $F(x)$. It is possible to see that eq. (20) to the influence function. This is possible starting from eq. (19) that can be written in general terms as:

$$\sum_{i=1}^{n}\psi(X_i;T)=0 \tag{41}$$

or:

$$\int \psi\left(x,T[F]\right)\mathrm{d}\,F=0\,. \tag{42}$$

The effect of the addicted arbitrary observation is:

$$\frac{\partial}{\partial\varepsilon}\int \psi\left(x,T\left[(1-\varepsilon)F+\varepsilon\,\delta_x\right]\right)\mathrm{d}\left[(1-\varepsilon)F+\varepsilon\,\delta_x\right]\Big|_{\varepsilon=0}=0\,, \tag{43}$$

which becomes, by changing the order of the integration and differentiation:

$$\int \psi\left(x,T\left[(1-\varepsilon)F+\varepsilon\,\delta_x\right]\right)\mathrm{d}\left[\,\delta_x-F\right]\Big|_{\varepsilon=0}+\int\frac{\partial}{\partial T[F]}\psi\left(x,T\left[(1-\varepsilon)F+\varepsilon\,\delta_x\right]\right)\times\frac{\partial}{\partial\varepsilon}T[F]\Big|_{\varepsilon=0}\mathrm{d}\,F\Big|_{\varepsilon=0}=0\,, \tag{44}$$

and simplifying:

$$\int \psi\left(x,T[F]\right)\mathrm{d}\left[\,\delta_x-F\right]+\frac{\partial}{\partial\varepsilon}T[F]\Big|_{\varepsilon=0}\times\int\frac{\partial}{\partial T[F]}\psi\left(x,T[F]\right)\mathrm{d}\,F=0\,, \tag{45}$$

Therefore, $IF(x,T,F)$ is also equal to:

$$IF(x,T,F)=\frac{\partial}{\partial\varepsilon}T[F]\Big|_{\varepsilon=0}=\frac{\psi\left(x,T[F]\right)}{-\int\frac{\partial}{\partial T[F]}\psi\left(x,T[F]\right)\mathrm{d}\,F}\,. \tag{46}$$

providing that the denominator is non-zero. Therefore the influence function is proportional to $\psi\left(x,T[F]\right)$:

$$IF(x,T,F)\propto\psi\left(x,T[F]\right)\,. \tag{47}$$

Now, a more precise definition of robustness can be introduced. The *gross error sensitivity* [8][13] is defined as:

$$\gamma(T,F)=\sup_x\left|IF(x,T,F)\right|\,. \tag{48}$$

If $\gamma(T,F)<+\infty$, the estimator is *robust* with respect to outliers, i.e. to anomalous values. In the case of LS, $\rho(e)=e^2$ and $\psi(e)=e$, thus the influence function is unbounded, while for the Huber' function $\gamma=c$ (see eq. (33)).

The robustness requires that the influence function is limited superiorly, but this requirement is in contrast to the estimator efficiency. This last property is instead often the target of the identification methods in mechanical systems [27]. In fact, a theorem presented in [13] states: let $X\sim F(x,\theta)$ and $T_n=T(X_1,X_2,\ldots,X_n)$ an estimator for θ and let $V_n'(\theta)$ the related score function. If T_n is Fisher's consistent, under regularity conditions

valid for Cramer-Rao's inequality, then T_n is efficient for θ if $IF(x,T,F) \propto V_n'(\theta)$. The *score function* is defined as:

$$V'(x;\theta) = \frac{\partial}{\partial\theta}\log f(x;\theta) = \frac{f'(x;\theta)}{f(x;\theta)}. \tag{49}$$

where f is the probability density function. The score function is normally unbounded, so that the influence function has to be both limited and unlimited (proportional to the score function) to achieve respectively estimator robustness and efficiency. To solve this paradox, the M-estimator class has been introduced and the tuning parameter takes into account the efficiency.

REFERENCES

[1] Andrews, D.F., Bickel, P., Hampel, F.R., Huber, P.J., Rogers, W.H. and Tukey, J.W. (1972): *Robust Estimates of Location: Survey and Advances*. Princeton Univ. Press, Princeton.

[2] Bachschmid, N. and Pennacchi, P. (2003): Accuracy of fault detection in real rotating machinery using model based diagnostic techniques", *JSME International Journal Series C*, **46**(3), pp. 1026-1034.

[3] Bachschmid, N., Pennacchi, P., Tanzi, E. and Vania, A. (2000): Accuracy of modelling and identification of malfunctions in rotor systems: experimental results. *Journal of the Brazilian Society of Mechanical Sciences*, **XXII**(3), pp. 423-442.

[4] Bachschmid, N., Pennacchi, P. and Vania, A. (2002): Identification of multiple faults in rotor systems. *Journal of Sound and Vibration*, **254**(2), pp. 327–366.

[5] Bachschmid, N., Pennacchi, P. and Vania, A. (2005): Robust fault identification in mechanical systems using M-estimators. Proc. of *ACIDCA-ICMI 2005*, Tozeur, Tunisia, Nov. 5-7, pp. 292-298.

[6] Bachschmid, N., Pennacchi, P., Vania, A., Zanetta, G.A. and Gregori, L. (2002): Case Studies of Fault Identification in Power Plant Large Rotating Machinery. Proc. of *IFToMM-6th International Conference on Rotor Dynamics*, Sydney, Australia, Sept. 30 – Oct. 3, pp. 191-200.

[7] Bachschmid, N., Pennacchi, P., Vania, A., Zanetta, G.A. and Gregori L. (2003): Identification of rub and unbalance in a 320MW turbogenerator. *International Journal of Rotating Machinery*, **9**(2) pp. 97-112.

[8] Bickel, P. (1983): Robust Estimation. In *Encyclopaedia of Statistical Sciences*, Eds. S. Kotz, N.L. Johnson, C.B. Read, N. Balakrishnan and B. Vidakovic, Vol. **8**, John Wiley & Sons, Ltd, pp. 157-163.

[9] Coleman, D., Holland, P., Kaden, N., Klema, V. and Peters, S.C. (1980): A system of subroutines for iteratively reweighted least squares computations. *ACM Trans. Math. Softw.*, **6**, pp. 327-336.

[10] Fox, J.: Robust regression, *An R and S-PLUS companion to applied regression*. http://cran.r-project.org/.

[11] Friswell, M.I. and Mottershead, J.E. (1995): *Finite Element Model Updating in Structural Dynamics*. Kluwer Academic Publishers, Dordrecht, The Netherlands.

[12] Hampel F.R., 1968, *Contributions on the Theory of Robust Estimation*, Ph.D. dissertation, University of California, Berkeley.

[13] Hampel, F.R., Ronchetti, E.M., Rousseeuw, P.J. and Stahel W.A. (1986): *Robust Statistics: The Approach Based on Influence Functions*, John Wiley, New York.

[14] Huber, P.J. (1981): *Robust Statistics*. John Wiley, New York.

[15] Jabr, R.A. (2005): Power system Huber M-estimation with equality and inequality constraints. *Electric Power Systems Research*, **74**(2), pp. 239-246.

[16] Krasker, W.S. (1983): Robust Regression. In *Encyclopaedia of Statistical Sciences*, Eds. S. Kotz, N.L. Johnson, C.B. Read, N. Balakrishnan and B. Vidakovic, **8**, John Wiley & Sons, Ltd, pp. 166-169.

[17] Mosteller F. and Tukey J.W., 1977, *Data Analysis and Regression*, Addison-Wesley, Reading, MA.

[18] Özyurt, D.B. and Pike R.W. (2004): Theory and practice of simoultaneous data reconciliation and gross error detection for chemical process. *Computers and Chemical Engineering*, **28**(3), pp. 381-402.

[19] Pennacchi, P., Bachschmid, N. and Vania, A. (2006): A model-based identification method of transverse cracks in rotating shafts suitable for industrial machines. *Mechanical Systems and Signal Processing*, doi:10.1016/j.ymssp.2005.04.005.

[20] Pennacchi, P., Bachschmid, N., Vania, A., Zanetta, G.A. and Gregori, L. (2006): Use of modal representation for the supporting structure in model based fault identification of large rotating machinery: part 1 – theoretical remarks. *Mechanical Systems and Signal Processing*, **20**(3), pp. 662-681.

[21] Pennacchi, P., Bachschmid, N., Vania, A., Zanetta, G.A. and Gregori, L. (2006): Use of modal representation for the supporting structure in model based fault identification of large rotating machinery: part 2 – application to a real machine. *Mechanical Systems and Signal Processing*, **20**(3), pp. 682-701.

[22] Pennacchi, P., Vania, A. and Bachschmid, N. (2006): Bivariate analysis of complex vibration data: an application to condition monitoring of rotating machinery. *Mechanical Systems and Signal Processing*, doi:10.1016/j.ymssp.2005.05.008.

[23] Platz, R., Markert, R. and Seidler M. (2000): Validation of Online Diagnostics of Malfunctions in Rotor Systems. Proc. of *IMechE-7th Int. Conf. on Vibrations in Rotating Machinery*, University of Nottingham, UK, 12-14 Sept., pp. 581-590.

[24] Rey, W.J.J. (1983): *Introduction to Robust and Quasi-Robust Statistical Methods*. Springer, Berlin.

[25] Rousseeuw, P.J. and Leroy, A.M. (1987): *Robust Regression and Outlier Detection*. John Wiley, New York.

[26] Tukey, J.W. (1975): Mathematics and picturing of data. *Proc. of International Congress of Mathematicians*, Vancouver, pp. 523-531.

[27] White, P.R., Tan, M.H. and Hammond, J.K. (2006): Analysis of the maximum likelihood, total least squares and principal component approaches for frequency response function estimation. *Journal of Sound and Vibration*, **290**(3-5), pp. 676-689.

[28] Yin, X. and Xie, M. (2003): Estimation of the fundamental matrix from uncalibrated stereo hand images for 3D hand gesture recognition. *Pattern Recognition*, **36**(3), pp. 567-584.

[29] Zhang, Z. (1997): Parameter estimation techniques: a tutorial with application to conic fitting, *Image and Vision Computing*, **15**(1), pp. 59-76.